Available online at www.sciencedirect.com
SCIENCE DIRECT®
PERGAMON
International Journal of Heat and Mass Transfer 46 (2003) 2993–3008
International Journal of HEAT and MASS TRANSFER
www.elsevier.com/locate/ijhmt

Formation characteristics of nitric oxide in a three-staged air/LPG flame

Han Seok Kim, Seung Wook Baek *, Myoung Jong Yu

Division of Aerospace Engineering, Department of Mechanical Engineering, Korea Advanced Institute of Science and Technology, 373-1 Kusung-dong, Yusung-gu, Taejon 305-701, South Korea

Received 31 January 2002; received in revised form 9 January 2003

Abstract

Experimental and numerical studies have been done to examine the effects of excess air ratio and tertiary air swirl number on the formation characteristics of NO in a pilot scale combustor adopting a multi-air staged burner. In numerical calculation the mathematical models for turbulence, radiation and nitric oxide chemistry were taken into account. The radiative transfer equation was solved using the discrete ordinates method with the weighted sum of gray gases model. In the NO chemistry model, the chemical reaction rates for thermal and prompt NO were statistically averaged using a probability density function. The results were validated by comparison with measurements. For the experiment, a 0.2 MW pilot multi-staged air burner has been designed and fabricated. Using the numerical simulation developed here, a variation of thermal and prompt NO formation was predicted by changing the excess air ratio and tertiary air swirl number. As the excess air ratio increased up to 1.9, the formation of the total as well as thermal NO at exit increased while the prompt NO decreased. The formation of thermal NO was more affected by concentration of O_2 and N_2 than gas temperature. When the tertiary air swirl number increased, the formation of the total as well as the prompt NO slightly decreased because of enhanced mixing of fuel and oxygen in the upstream reaction zone and reduced gas temperature at exit.

Keywords: Radiation; Three-staged air/LPG flame; Excess air ratio; NO formation; Swirl number

1. Introduction

Nowadays, due to increasing concerns over the environmental pollution, a development of NO_x reduction method has become an imminent problem to be installed in combustion devices. The nitric oxide, NO is usually formed from atmospheric nitrogen during the combustion process of hydrocarbon and air through two mechanisms. Firstly, it, usually termed as the thermal NO, is the Zeldovich chain reaction which dominantly depends on its local temperature and reactants, while the second mechanism, so-called the prompt NO, is produced through CH radical reaction with molecular nitrogen for fuel rich case [1].

Among many other effective ways to control the NO emission, the air staged combustion technique is implemented in many fossil fuel-fired combustion systems, since its combustion chamber is easily adapted for its use. In upstream of air staged-burner a theoretically lesser amount of air is supplied, while the remaining air is supplied farther downstream via staged air nozzles. However, its mixing and combustion characteristics are not so well understood that its practical application to the burner is still limited. In this type of burner the aerodynamic mechanism plays a significant role in producing fuel-rich or lean region in flame.

Smart and Webber [2] exerted a great deal of efforts to investigate the effects of swirl number and flow velocity on its aerodynamic characteristics. A NO formation in

* Corresponding author. Tel.: +82-42-869-3714; fax: +82-42-869-3710.
E-mail address: swbaek@sorak.kaist.ac.kr (S.W. Baek).

0017-9310/03/$ - see front matter © 2003 Elsevier Science Ltd. All rights reserved.
doi:10.1016/S0017-9310(03)00067-X

Nomenclature

E_b	blackbody emissive power, W/m^2
I	radiation intensity, W/(m^2 sr)
Nu	Nusselt number
q	heat flux, W/m^2
R	reaction rate, kg/m^3/s
r	coordinate direction or radius, m
$\hat{s}$	angular direction
s	distance traveled
S	swirl number
t	time, s
T	temperature, K
u	axial velocity, m/s
v	radial velocity, m/s
V	volume, m^3
w	weighting factor in WSGGM or tangential velocity, m/s
W	molecular weight, kg/kmol
x	coordinate direction
Y_i	mass fraction

Greek symbols

λ	excess air ratio
ε	emissivity
κ	absorption coefficient, 1/m
σ	Stefan–Boltzmann constant, 5.67×10^{-8} W/(m^2 K^4)
ρ	density, kg/m^3
μ, ξ	direction cosine in the x and r direction

Superscript

$'$	incident direction

Subscripts

b	blackbody
c	centerline
g	gas
w	wall
η	wave number
ox	oxygen
p	product
fu	fuel
re	reference

natural gas combustion with multi-staged air has been experimentally examined by Toqan et al. [3]. The radial flame stratification was found to reduce a degree of air/fuel mixing and thereby, yield a moderate distribution of gas temperature and NO emission. Shihadeh et al. [4] parametrically studied the effects of swirl number and external air staging to investigate the feasibility of aerodynamic staging for low NO_x combustion using heavy fuel oil, of which results were then applied to boiler and gas turbine [5]. Using commercial code, Fluent, Sun [6] performed a numerical analysis to investigate a flame structure in multi-staged natural gas flame. Although its numerical result was not in so good agreement with experiments, its trend with aerodynamic changes was reasonably accurate.

In this study, an experimental as well as numerical study has been carried out to investigate an influence of the excess air ratio and tertiary air swirl number on thermal and prompt NO production in a pilot scale combustor that adopts the air-staged LPG flame. The numerical prediction has been done by means of establishing appropriate mathematical models for turbulence, turbulent combustion, thermal radiation and nitric oxide chemistry. The radiative transfer equation (RTE) was solved using the discrete ordinates method (DOM) with the weighted-sum-of-gray-gases model (WSGGM) that accounts for the non-gray gas effects by CO_2 and H_2O. Thermal NO and prompt NO chemical reaction rates were statistically averaged using the β probability density function (pdf). Experimental measurements were also made when the liquefied petroleum gas (LPG) was injected. The numerical results were then validated in comparison with the experimental data. Based on this validation, the effects of excess air ratio and tertiary air swirl number on the characteristics of thermal and prompt NO formation were analyzed and discussed.

2. Experiments

In Fig. 1, a schematic of three air-staged LPG burner with a capacity of 0.2 MW is illustrated. For the purpose of industrial high-capacity it is usually designed and constructed to generate a long flame. The fuel nozzle is of hollow cone type with jet angle of 30° of which flow rate is monitored using a calibrated orifice flowmeter. The staged combustion air is supplied through a calibrated air flowmeter to the primary, secondary and tertiary air nozzles which are concentrically placed. For flame stabilization one swirler with vane angle 60° is coaxially installed in the primary nozzle, while another one with vane angle 30°, 45° or 60° is positioned in the tertiary nozzle to investigate the influence of tertiary air swirl number.

Fig. 2 represents a schematic of experimental combustor. Its system comprises burner, fuel supply and blower. The furnace is 3.5 m long and 0.7 m in diameter. The furnace wall temperature is adjusted by partially

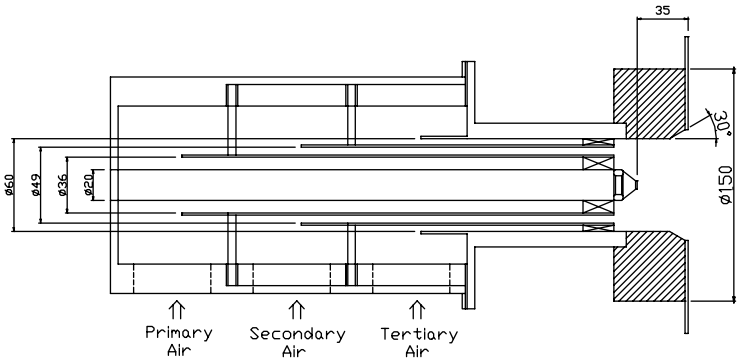

Fig. 1. Dimensional configuration of the multi-staged air burner.

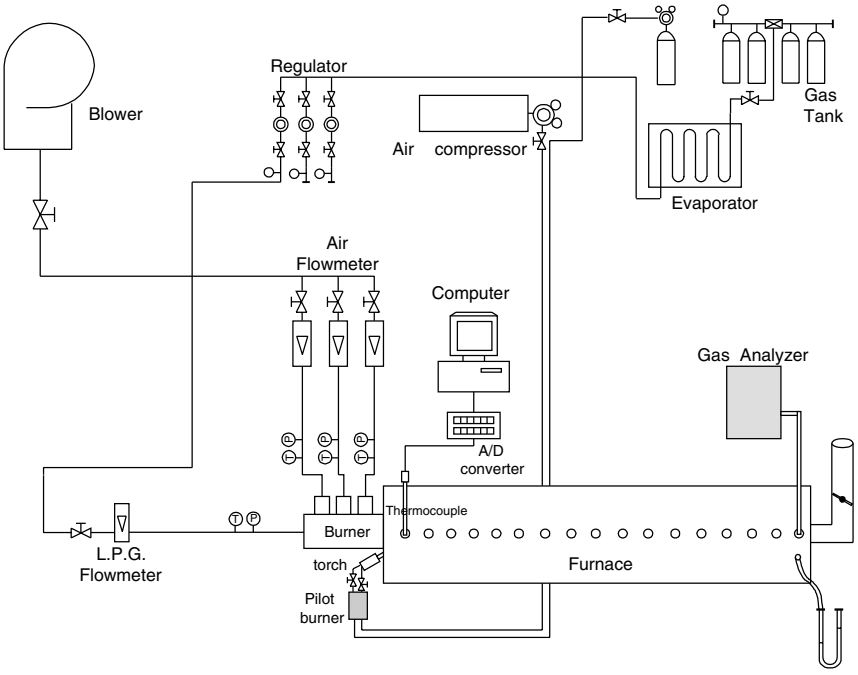

Fig. 2. Schematic diagram of experimental equipment.

setting up water cooling pipe around the wall. Remaining part of the furnace wall is insulated using ceramic wool with thickness of 50 mm. The U-shaped tube manometer monitors the pressure inside the furnace. In order to measure the temperature and species concentrations in combustor, inspection holes (ϕ 25.4 mm) are made every 100 mm along the axial direction of the furnace wall. The sample gases are taken using a water-cooled stainless steel probe. Through water trap the samples are dried and analyzed for CO, NO, NO_2, and O_2 using the Gas Analyzer (Greenline MK2).

The gas temperature is measured with a bare-wire Pt/13% Rh–Pt thermocouple, which is sheathed in straight length of twin-bore ceramic cladding of 5 mm-o.d. The thermocouples are calibrated with Isotec/877 in 400–1100 °C range. Within calibration range, the measurement error in temperature is less than 1%. The thermocouple signals are recorded using a PLC-812PC board with 12 bit and PCL-889 screw terminal (Advantech Co.). For the radiative correction, three types of bead, 75, 100 and 120 μm in diameter are used [7]. The gas concentration and temperature are measured at every 2.5 cm in radial direction by traversing equipment through the inspection holes. All the measurements are time-averaged for the operating conditions given in Table 1.

Table 1
Experimental conditions

Fuel mass flow rate	15.2 kg/hr
Fuel jet angle	30°
Excess air ratios (air flow rate)	1.1(260 kg/hr), 1.3(307 kg/hr) 1.5(354 kg/hr), 1.9(449 kg/hr)
Primary, secondary, tertiary air flow rates	20%, 45%, 35%
Primary air stage vane angle (swirl number)	60° ($S = 1.38$)
Secondary air stage vane angle	0°
Tertiary air stage vane angles (swirl number)	30° ($S = 0.54$), 45° ($S = 0.93$), 60° ($S = 1.62$)
Combustion air temperature	50 °C
Cooling water temperature (in/out)	21/92 (°C)
Cooling water flow rate	1200 kg/hr
Pressure field of furnace	+ 20 N/m^2 (gauge pressure)

3. Numerical analysis

3.1. Mathematical model

As previously mentioned in experiments, a partially upstream section of the furnace wall is water-cooled so that it is assumed constant temperature, while the remaining part of furnace wall is insulated using adiabatic ceramic wool. To numerically predict thermo-chemical characteristics, a two-dimensional axisymmetric mathematical model is to be introduced. It comprises the overall mass continuity, momentum equation for axial, radial and tangential directions, energy equation, turbulence model and chemical species conservation equation, all of which can be written in the following generalized form

$$\frac{\partial(\rho U\Phi)}{\partial x}+\frac{1}{r}\frac{\partial(r\rho V\Phi)}{\partial r}=\frac{\partial}{\partial x}\left(\Gamma_\varphi\frac{\partial\Phi}{\partial x}\right)+\frac{1}{r}\frac{\partial}{\partial r}\left(r\Gamma_\varphi\frac{\partial\Phi}{\partial r}\right)+S_\varphi \qquad (1)$$

where $\Phi = 1$ represents the continuity equation, while a substitution of u, v and w into Φ generates the momentum equation for each respective direction. The conservation equations for the species mass fraction and the enthalpy can be obtained when the mass fraction, Y_i or the mixture enthalpy, h, is substituted into Φ. Γ_φ is the diffusion coefficient and S_φ is the source or sink term for the variable Φ. The thermo-physical properties are represented by a function of temperature based on the experimental data [8]. The effective turbulent viscosity is calculated by $\mu_{\text{eff}} = \mu_l + C_\mu\rho k^2/\varepsilon$ where μ_l is laminar viscosity and $C_\mu = 0.09$ by employing the standard k–ε model. In near wall region the wall function is used, since the viscous effect is dominant [9]. The equations above are numerically solved by modifying the conventional TEACH code [10].

3.2. Radiative heat transfer

For a specific direction, l, the RTE for absorbing and emitting gray gas in cylindrical coordinate can written by

$$\mu_l\left(\frac{\partial I^l}{\partial x}\right)+\frac{\xi^l}{r}\frac{\partial(rI^l)}{\partial r}-\frac{1}{r}\frac{\partial(\eta^l I^l)}{\partial\psi}=-\kappa I^l+\kappa I_b \qquad (2)$$

where κ, I^l, and I_b are the absorption coefficient, directional intensity and black body radiation intensity, respectively. $\mu^l = \cos\theta$, $\xi^l = \sin\theta\cos\psi$ and $\eta^l = \sin\theta\sin\psi$ are axial, radial and tangential direction cosines. In this study, DOM is chosen to solve RTE, the angular integration is approximated by quadratic summation such that

$$\int_{4\pi} I\,d\Omega=\sum_{l=1}^{L} I^l w^l \qquad (3)$$

where w^l is the angular weights for corresponding directional intensity.

Since the gas species such as CO_2 and H_2O have non-gray gas effects, DOM is combined with the WSGGM. Then the RTE can be written for kth gray gas such that

$$\mu_l\left(\frac{\partial I_k^l}{\partial x}\right)+\frac{\xi^l}{r}\frac{\partial(rI_k^l)}{\partial r}-\frac{1}{r}\frac{\partial(\eta^l I_k^l)}{\partial\psi}=-\kappa_k I_k^l+\kappa_k w_k I_b \qquad (4)$$

where κ_k, I_k, and w_k are the absorption coefficient, directional intensity and weighting factor for kth gray gas respectively. For CO_2/H_2O/clear-gas mixture, Smith et al. [11] used a third order polynomial to represent the weighting factors in Eq. (4) for the kth gray gas component, based on the gas temperature, T_g can be such that

$$w_k(T_g)=\sum_{j=1}^{4} b_{\varepsilon,k,j}T_g^{j-1} \qquad (5)$$

$$\sum_{k=1}^{4} w_k(T_g) = 1 \tag{6}$$

where $b_{\varepsilon,k,j}$ are referred to as the emissivity gas temperature polynomial coefficients. And absorption coefficients, κ_k, are also can be found in Smith et al. [11].

The total intensity I can be calculated by summing up all the kth gray gas intensities such that

$$I = \sum_k I_k \tag{7}$$

The divergence of the radiative heat flux in the energy conservation equation is then denoted by [12]

$$-\nabla \cdot q_r = -\sum_k \nabla \cdot q_{r,k} = \sum_k \kappa_k \left[\int_{4\pi} I_k(r,\Omega)\,\mathrm{d}\Omega - 4\pi w_k I_b \right] \tag{8}$$

where Ω is the solid angle.

3.3. Chemical reaction

Since a main ingredient of LPG used in this experiment is propane (95%), the reaction is assumed as a two-step mechanism as follows;

$$C_3H_8 + \tfrac{7}{2}O_2 \rightarrow 3CO + 4H_2O \tag{R-1}$$

$$CO + \tfrac{1}{2}O_2 \rightarrow CO_2 \tag{R-2}$$

The source or sink term due to combustion, S_φ, in the species conservation equation can be modeled using the eddy dissipation model [13] so that the reaction rates of C_3H_8 and CO are considered to be proportional to turbulence time scale (ε/k) as well as to the smallest of the fuel, oxygen, carbon monoxide or product concentrations.

The reaction rate for (R-1) is then represented by

$$R_{fu} = \rho \frac{\varepsilon}{k} \min\left\{ aY_{fu}, a\frac{Y_{ox}}{s_1}, b\frac{Y_p}{1+s_1} \right\} \tag{9}$$

while the reaction rate for (R-2) becomes

$$R_{CO} = \rho \frac{\varepsilon}{k} \min\left\{ aY_{CO}, a\frac{Y_{ox}}{s_2}, b\frac{Y_{CO_2}}{1+s_2} \right\} \tag{10}$$

where s_1 and s_2 are the stoichiometric mass ratio of oxygen to fuel and CO, respectively and empirical constants of $a = 3.5$, $b = 2$ are used for the eddy dissipation model [14].

The chemical reaction involved in the NO formation may be decoupled from the other species, since the amount of NO formed is small and the reaction of NO formation by thermal mechanism is generally slow compared with the fuel oxidation. Therefore, the NO concentration is post-calculated after the velocity, temperature, turbulence, and major species concentration are obtained. Prompt as well as thermal NO kinetics is considered here. Eq. (1) for NO formation in axi-symmetric coordinate may be written by

$$\frac{\partial(\rho u Y_{NO})}{\partial x} + \frac{1}{r}\frac{\partial(r\rho v Y_{NO})}{\partial r} = \frac{\partial}{\partial x}\left(\Gamma_{NO}\frac{\partial Y_{NO}}{\partial x}\right) + \frac{1}{r}\frac{\partial}{\partial r}\left(r\Gamma_{NO}\frac{\partial Y_{NO}}{\partial r}\right) + \overline{S}_{NO} \tag{11}$$

The time-averaged NO formation, $\overline{S}_{NO}$, is independently determined for both thermal and prompt NO, whereas the fuel NO kinetics is neglected in this calculation since LPG has a negligible nitrogen compound. Among others, Peters and Weber's approach [15] is used here for estimation of $\overline{S}_{NO}$ in turbulent flame.

For a fuel lean or near-stoichiometric mixture, Zeldovich proposed the following principal reactions that govern the formation of thermal NO

$$O + N_2 \overset{k_{1f},k_{1b}}{\leftrightarrow} NO + N \tag{R-3}$$

$$N + O_2 \overset{k_{2f},k_{2b}}{\leftrightarrow} O + NO \tag{R-4}$$

For a fuel rich and near-stoichiometric mixture, the reaction

$$N + OH \overset{k_{3f},k_{3b}}{\leftrightarrow} NO + H \tag{R-5}$$

additionally contributes to the formation of thermal NO [16] so that the combined reactions of R-3, R-4, R-5 are usually referred to as the extended Zeldovich mechanism.

By assuming that N atom concentration is steady state and that the reactions of R-3, R-4 are dominant, the reaction rate of thermal NO formation can be written as

$$\frac{\mathrm{d}[NO]_t}{\mathrm{d}t} = \frac{2[O](k_{1f}k_{2f}[O_2][N_2] - k_{1b}k_{2b}[NO]^2)}{k_{2f}[O_2] + k_{1b}[NO]} \tag{12}$$

where $[X_i]$ is mole fraction of species i, k_{1f}, k_{1b}, k_{2f} and k_{2b} are forward and backward rate constants which are the following expressions in $cm^3/g\,mol$ [15];

$$\begin{aligned} k_{1f} &= 7.6\times10^{13}\exp(-75514/RT);\\ k_{1b} &= 1.6\times10^{13};\\ k_{2f} &= 6.4\times10^{9}T\exp(-6260/RT);\\ k_{2f} &= 1.5\times10^{9}T\exp(-38650/RT). \end{aligned} \tag{13}$$

O-radicals concentration in Eq. (12) is assumed to be equal to the equilibrium O-radicals concentration as in the case of molecular oxygen dissociation [15].

The source or sink of thermal NO formation (S_{t-NO}) is then expressed by

$$S_{t-NO} = W_{NO}\frac{d[NO]_t}{dt} \tag{14}$$

For the case of hydrocarbon combustion, Fenimore [1] suggested a following reaction mechanism for the prompt NO formation

$$CH + N_2 \leftrightarrow HCN + N$$

$$C + N_2 \leftrightarrow CN + N$$

Based on these, De Soete [20] proposed a following chemical reaction rate for prompt NO formation

$$\frac{d[NO]_p}{dt} = C\frac{W^{1+b}}{\rho^{1+b}}[O_2]^b[N_2][C_xH_y]\exp\left(-\frac{E_a}{RT}\right) \tag{15}$$

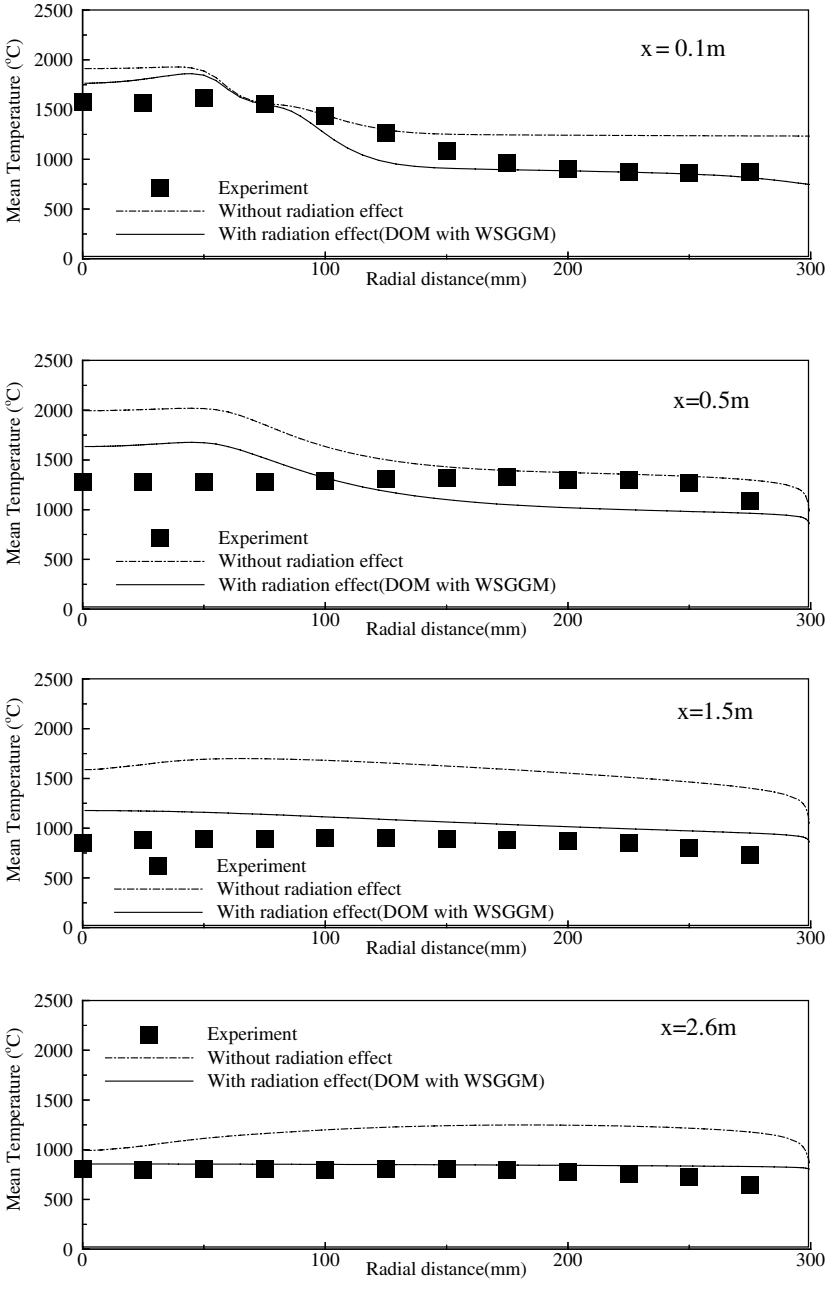

Fig. 3. Radial temperature distribution at various axial locations. (excess air ratio = 1.1, $S_{primary} = 1.38$, $S_{tertiary} = 0.54$).

$$S_{\mathrm{p-NO}} = W_{\mathrm{NO}} \frac{\mathrm{d}[\mathrm{NO}]_{\mathrm{p}}}{\mathrm{d}t} \tag{16}$$

where $C = 6.4 \times 10^6\ \mathrm{s}^{-1}$, $E_{\mathrm{a}} = 3.038 \times 10^8$ J/kmol and $b = 0.5$.

Since a practical flame is highly turbulent, a statistical method is chosen here so that a pdf is used to estimate the average value of the NO reaction rate. In this study only the temperature is used as a single variable of pdf for the NO reaction rate, for it is strongly temperature dependent [17].

With Beta-pdf, the source term, $\overline{S}_{\mathrm{NO}}$, in the governing equation for NO formation can be expressed by [15]

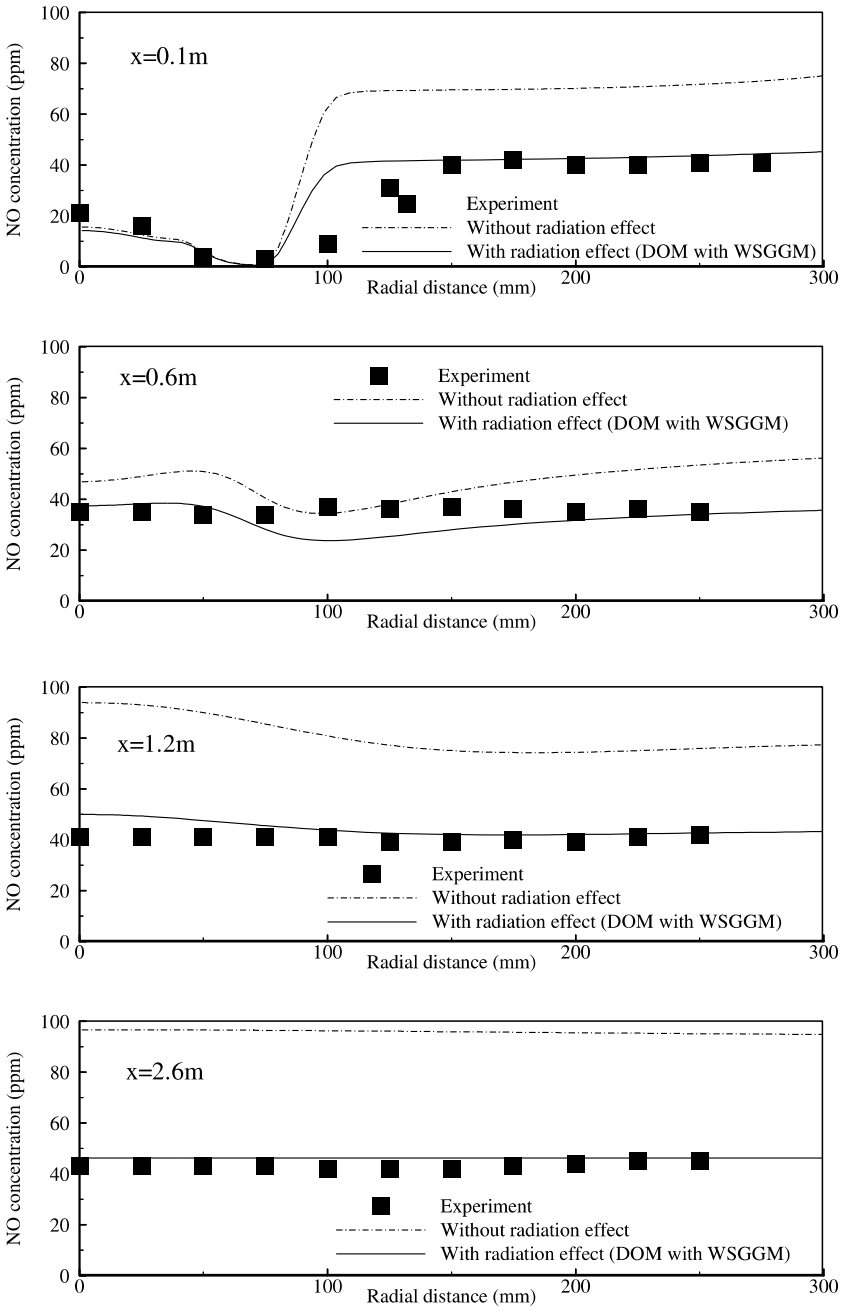

Fig. 4. Radial profiles of NO at various axial locations. (excess air ratio = 1.1, $S_{\mathrm{primary}} = 1.38$, $S_{\mathrm{tertiary}} = 0.54$).

$$\overline{S}_{NO} = \overline{S}_{t-NO} + \overline{S}_{p-NO} = W_{NO}\int_{T_{min}}^{T_{min}+\Delta T}\left\{\frac{d[NO]_t}{dt}+\frac{d[NO]_p}{dt}\right\}\beta_{pdf}(T) \times \frac{dT}{T_{max}-T_{min}} + \frac{W_{NO}}{N}\sum_{i=2}^{N-1}\left\{\frac{d[NO]_t}{dt}+\frac{d[NO]_p}{dt}\right\} \times (T_{mi})\beta_{pdf}(T_{mi}) \quad (17)$$

$$T_{mi} = T_{min} + \frac{2i-1}{2}\Delta T, \quad \Delta T = \frac{T_{max}-T_{min}}{N} \quad (18)$$

where $\beta_{pdf}(T)$ is the beta probability function of temperature. T_{max} and T_{min} are the highest-possible and lowest-possible values of the instantaneous temperature, and N denotes the number of integration intervals.

3.4. Boundary conditions

The following adiabatic boundary condition is used for the furnace wall covered by ceramic wool

$$-C_p\left(\frac{\mu_l}{Pr_l}+\frac{\mu_t}{Pr_t}\right)\frac{\partial T}{\partial x_i}\bigg|_w + q_{r,x_i}|_w = 0 \quad (19)$$

where the first term on the left hand side is the net conductive heat flux at wall while the second term is the net radiative heat flux leaving the wall surface.

Regarding the RTE, all the boundaries are assumed gray and diffuse. Along the water-cooled section of the furnace, the constant wall temperature is assumed so that the following wall boundary condition is used

$$I_{k,w} = \varepsilon_w w_k I_B + \frac{1-\varepsilon_w}{\pi}\sum_{\mu^{l'}<0} I_k^{l'}|\mu^{l'}|\Omega^{l'} \quad (20)$$

where the first term on the right hand side represents the emission at its local wall temperature, whereas the second term accounts for reflection of all the incoming radiative intensities, $I_k^{l'}$, coming from the incoming $\mu^{l'} < 0$ directions. The ceramic wool section of the furnace wall is adiabatic so that the wall boundary condition becomes [18]

$$I_{k,w} = \frac{1}{\pi}\left(\sum_{\mu^{l'}<0} I_k^{l'}|\mu^{l'}|\omega^{l'} - w_{g,k}(T_w)C_p\left(\frac{\mu_l}{Pr_l}+\frac{\mu_t}{Pr_t}\right)\frac{\partial T}{\partial x_i}|_w\right) \quad (21)$$

At the axi-symmetric axis it becomes

$$I_{k,w}^{l} = I_{k,w}^{l'} \quad (22)$$

for $|\mu^{l}| = |\mu^{l'}|$ and $\xi^{l} = -\xi^{l'}$ at $r = 0$.

4. Results and discussion

4.1. Validation of numerical results

Based on the preliminary calculations considering computational time and numerical accuracy, a non-uniform grid system of 93×91 is adopted to numerically analyze the multi-staged air/LPG flame. Computationally, the quarl section is constructed using a step boundary. In the below the computational results for thermal and chemical characteristics are discussed and validated by comparison with experimental data for the excess air ratio, $\lambda = 1.1$. Then, the formation characteristics of thermal as well as prompt NO are examined for various excess air ratios and tertiary air swirl numbers.

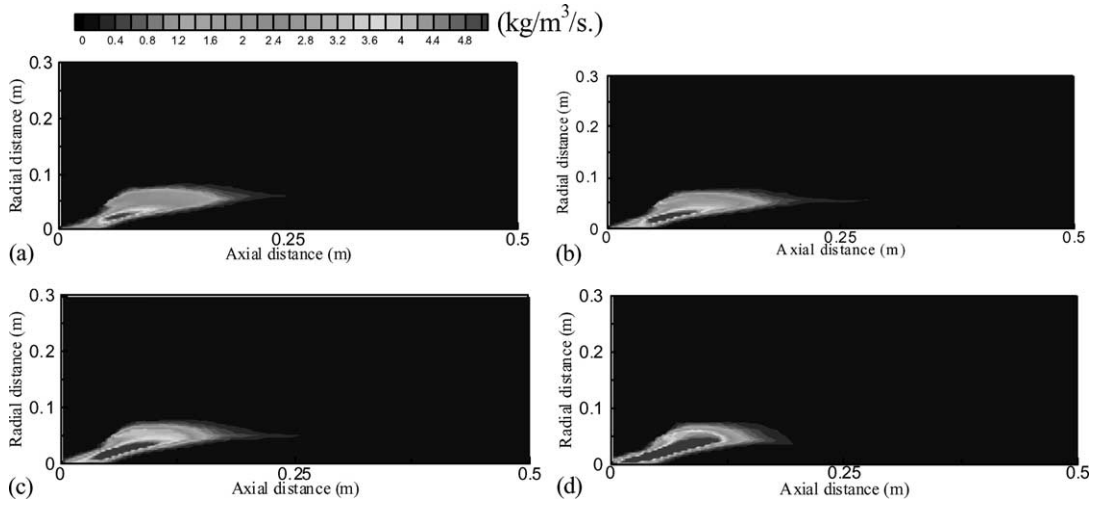

Fig. 5. Reaction rate of fuel, kg/m^3/s. Excess air ratio: (a) 1.1, (b) 1.3, (c) 1.5 and (d) 1.9.

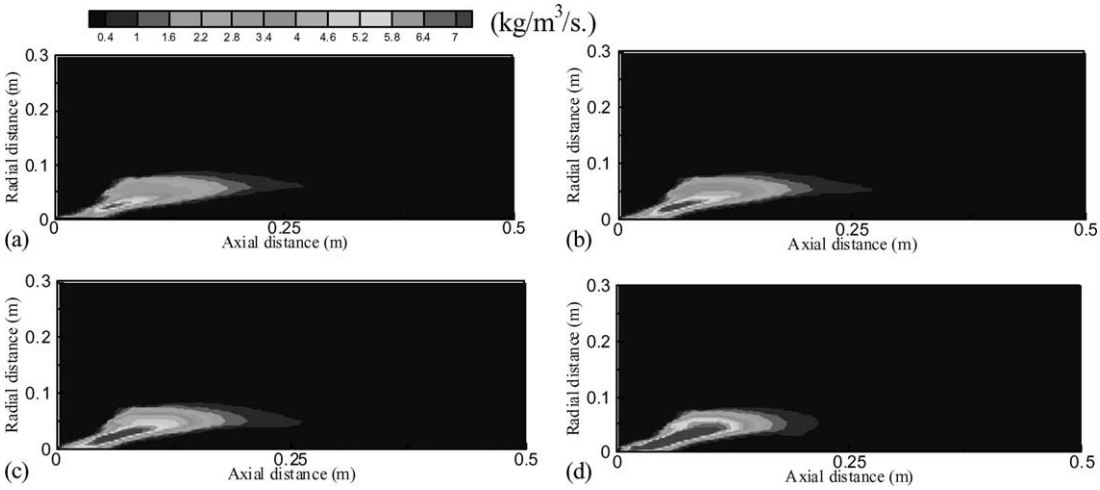

Fig. 6. Reaction rate of CO, kg/m^3/s. Excess air ratio: (a) 1.1, (b) 1.3, (c) 1.5 and (d) 1.9.

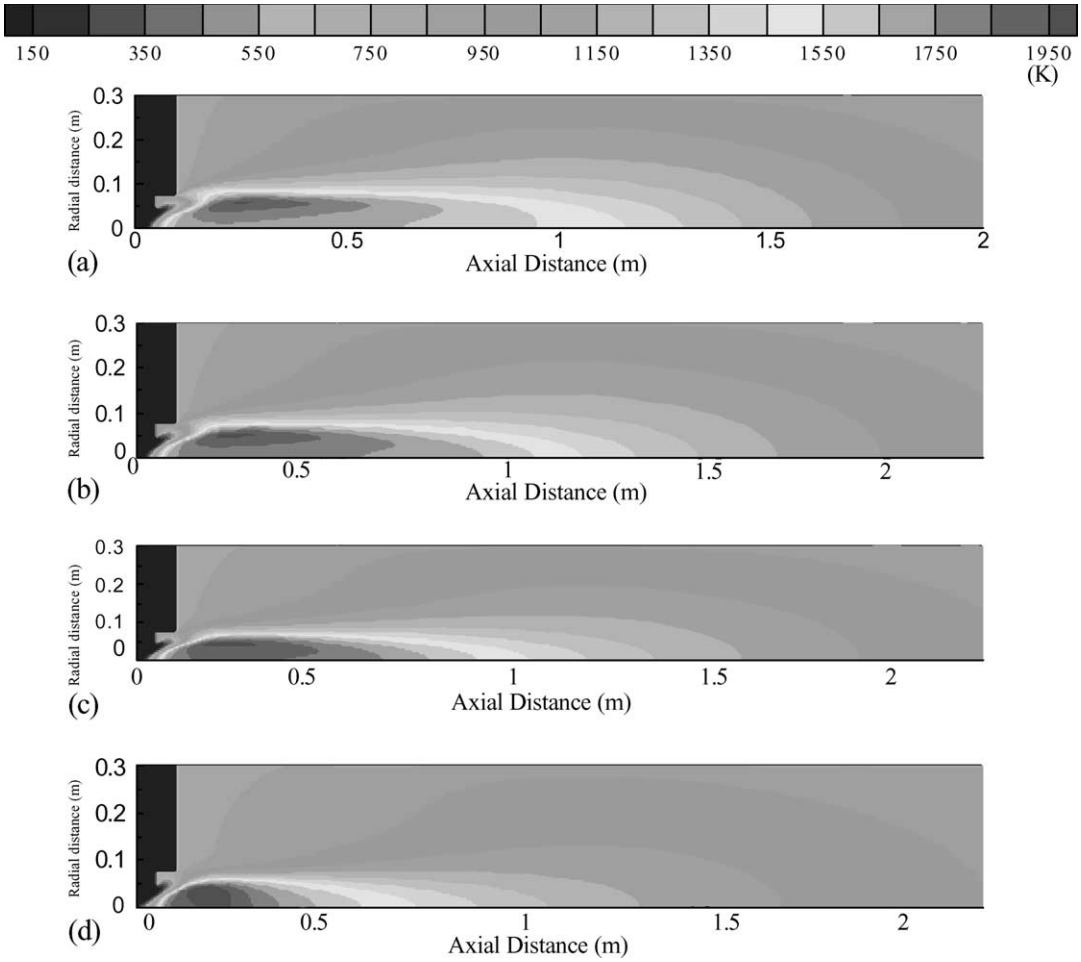

Fig. 7. Predicted isothermal lines for various excess air ratios, K. Excess air ratio: (a) 1.1, (b) 1.3, (c) 1.5 and (d) 1.9.

4.1.1. Temperature distribution

In Fig. 3 the measured radial temperature distributions are plotted at four axial locations of 0.1, 0.5, 1.5, and 2.6 m and compared with two numerical results for the condition of excess air ratio, $\lambda = 1.1$ and primary and tertiary air swirl number, $S_{\text{primary}} = 1.38$, $S_{\text{tertiary}} = 0.54$. Some divergence is observed for the radial temperature distribution at $x = 0.5$ m where the cooling pipe is wrapped around the furnace wall. This is due to the fact that experimentally the cooling pipe is placed inside the furnace, whereas the wall is considered smooth in the calculation. Nonetheless, in overall the temperature variation obtained by using DOM with WSGGM and pertinent boundary conditions for radiation is satisfactory compared with the experimental ones.

4.1.2. NO distribution

Radial variation of NO at $x = 0.1$, 0.6, 1.2 and 2.6 m is plotted and compared with measurements in Fig. 4. According to Drake et al. [19] a little portion of the NO at reaction zone is converted to NO_2 during sampling so that actually the total concentration of NO as well as NO_2 is measured in experiment while only NO is predicted in the numerical calculation. As noted in the Fig. 4, when the radiation effect is neglected in the calculation, the predicted NO exceeds the measured one since its temperature is also higher as shown in Fig. 3. On the other hand, when the radiation effects are taken into consideration, there is only a small deviation between the numerical and experimental results at $x = 0.1$ and 0.6 m, while its difference becomes much smaller at $x = 1.2$ and 2.6 m. Therefore, the thermal and prompt

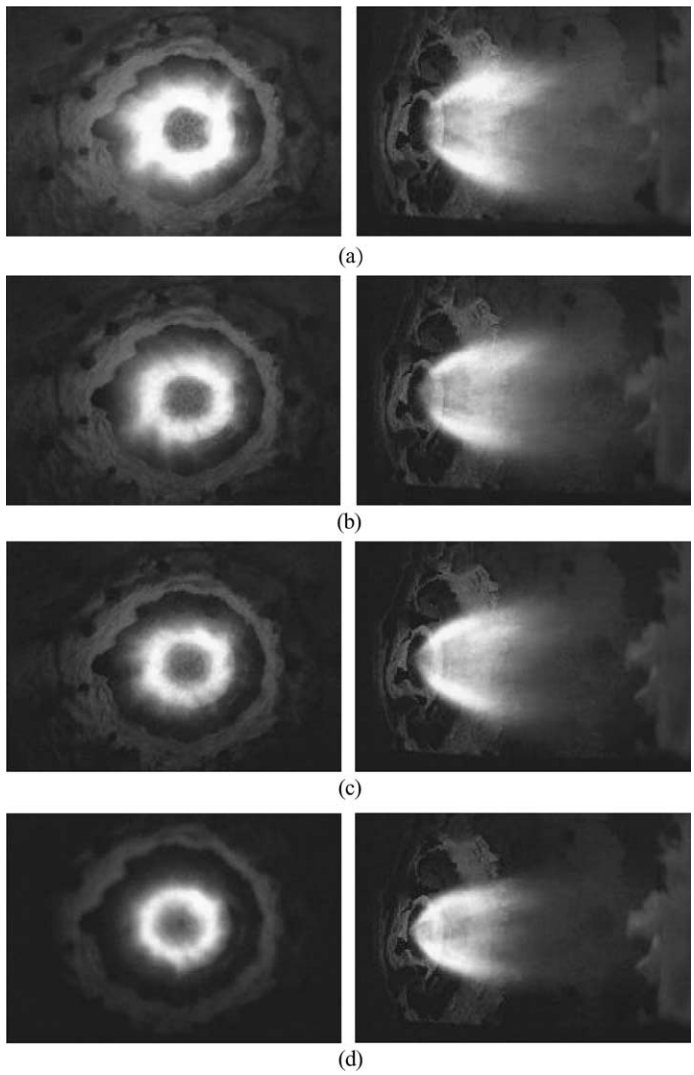

Fig. 8. Photographs of flame for various excess air ratios. Excess air ratio: (a) 1.1, (b) 1.3, (c) 1.5 and (d) 1.9.

NO chemistry models used in this study, which are based on the oxygen and temperature distributions with necessary empirical constants, are considered quite appropriate for numerical modeling of NO formation by applying the DOM with WSGGM for radiation.

4.2. Effects of excess air ratio

4.2.1. Reaction rate and temperature

Variations of reaction rate of fuel (LPG) and carbon monoxide (CO) with the excess air ratio are plotted in Figs. 5 and 6. As shown in Fig. 5, as the excess air ratio increases, the peak depletion zone of fuel (red-colored zone in the figure) becomes broader while its overall size of reaction zone slightly decreases due to its increasing concentration of oxygen. Similarly, the peak production rate of CO becomes also broader as the excess air ratio increases as in Fig. 6. A variation of gas temperature with excess air ratio is numerically calculated and plotted in Fig. 7. The size of high temperature region is seen to shrink and get closer to the burner inlet as the excess air ratio increases. This fact is also observed in experimental photographs of flame as shown in Fig. 8. The left-hand side photo is taken from the end-section of the combustor, while the right-hand side photo is the side

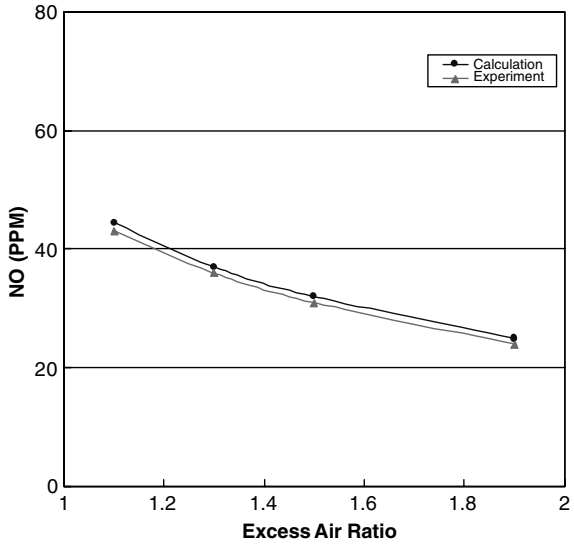

Fig. 9. Comparison between prediction and measurement of total NO volumetric percent for various excess air ratios.

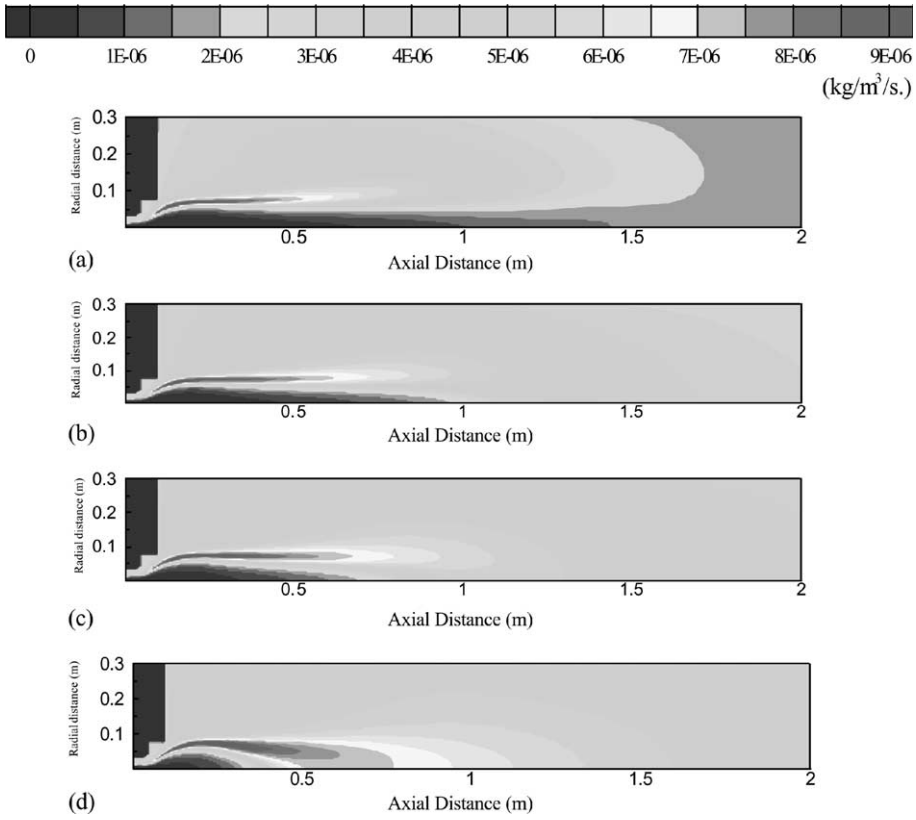

Fig. 10. Production rate of thermal NO for various excess air ratios, kg/m^3/s. Excess air ratio: (a) 1.1, (b) 1.3, (c) 1.5 and (d) 1.9.

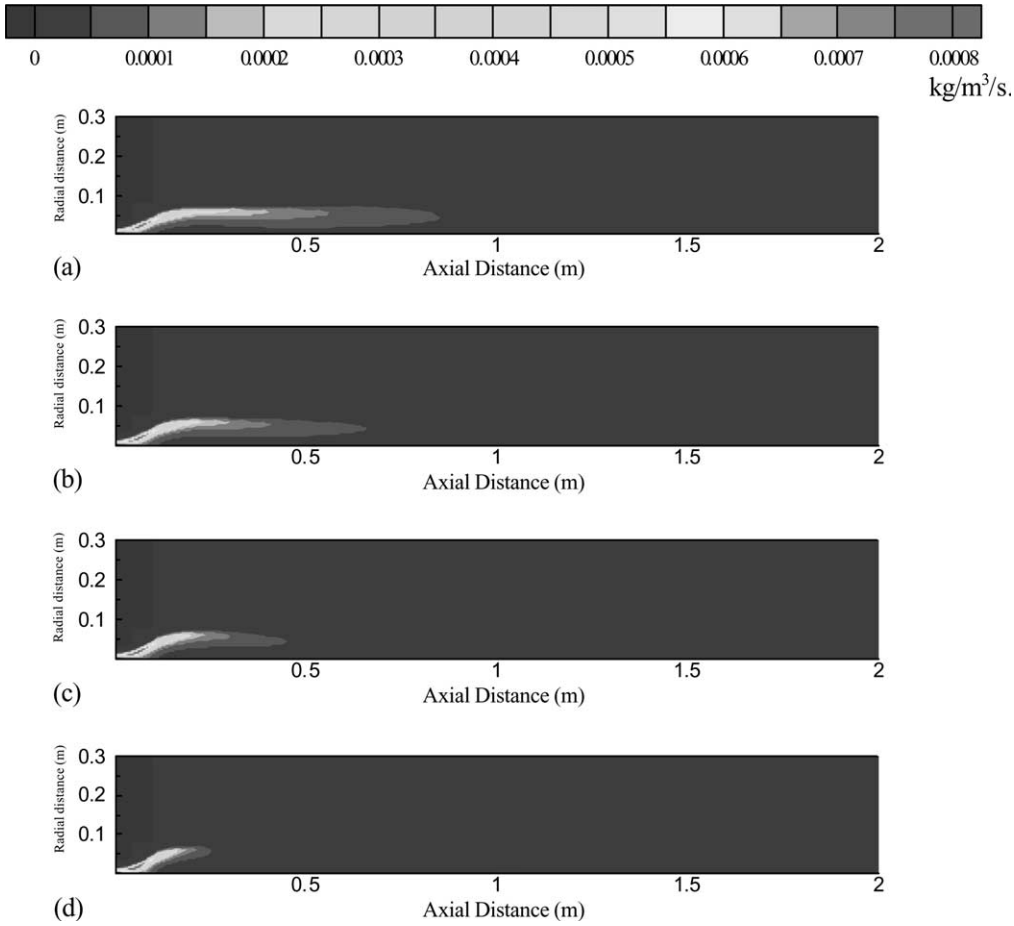

Fig. 11. Production rate of prompt NO for various excess air ratios, kg/m^3/s. Excess air ratio: (a) 1.1, (b) 1.3, (c) 1.5 and (d) 1.9.

view of the flame. Consequently, the qualitative change in experimental flame shape with excess air ratio is in good agreement with numerical results.

4.2.2. NO formation

The computed and measured emissions of total NO at exit of the combustor are compared in Fig. 9 when the excess air ratio is varied. The computed NO emission, as a whole, shows a good agreement with the experimental data. In Fig. 9, even though the volumetric percent of NO decreases at the exit as the excess air increases, it must be noted that the total formation of NO actually increases, since more air is supplied.

In Figs. 10 and 11, a spatial distribution of the thermal and prompt NO formation is numerically obtained and depicted, in which the colored-scale in Fig. 11 is three orders of magnitude larger than that in Fig. 10. It is noted that the source of prompt NO is much higher than that of thermal NO at the flame front as a whole. This results from the fact that the prompt NO is created from CH radical, which is formed as an intermediate at flame front only, so that the prompt NO is primarily generated at the flame front. Therefore, the NO concentration at $x = 0.1$ m observed in Fig. 4 is considered to mainly originate from prompt NO generation. On the other hand, it is seen in Fig. 10 that the thermal NO is produced in broad region while most of them are distributed at a high temperature region exceeding 1200 K, based on the Zeldovich reaction mechanism.

According to Figs. 10 and 12, the formation of thermal NO is still higher and produced across broader region even though the gas temperature decreases as the excess air increases. As a result, it can be considered that the formation of thermal NO is more affected by concentration of O_2 and N_2 than the gas temperature in the range of excess air ratio given here. The reason could not be exactly analysed now, because owing to many difficulties, the currently available NO prediction strategies still have a degree of uncertainty. However, the forma-

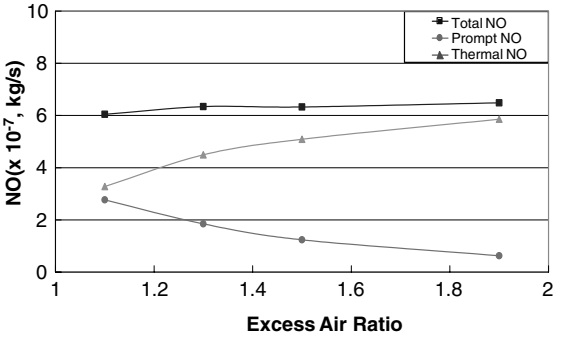

Fig. 12. Total production of thermal and prompt NO for various excess air ratios, kg/s.

tion of prompt NO is seen to decrease in Fig. 11 due to its decreasing fuel rich zone as the excess air increases, because the prompt NO is mainly formed in fuel rich zone.

The formations of total, thermal and prompt NO generated in the whole combustor are plotted and compared for various excess air ratio in Fig. 12. As the excess air increases, the formation of thermal NO increases, while the prompt NO decreases. Consequently, the total formation of NO is observed to slightly increase as the excess air ratio increases for the given excess air ratios.

4.3. Effects of swirl number of tertiary staged air

4.3.1. Temperature

In Fig. 13 the gas temperature variations with tertiary air swirl number are shown for the case of excess air ratio, $\lambda = 1.1$. It must be noted that the total amount of tertiary air supplied is not changed while its swirl number is varied. As the tertiary air swirl number increases, the isothermal lines are seen to shift a little towards upstream direction. Therefore, the tertiary air with higher swirl number is considered to enhance the

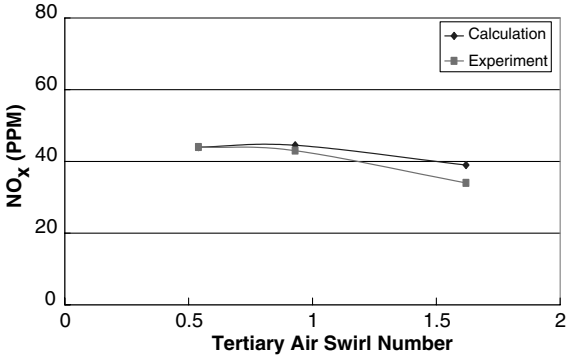

Fig. 14. Comparison between prediction and measurement of total NO volumetric concentration for various tertiary air swirl numbers.

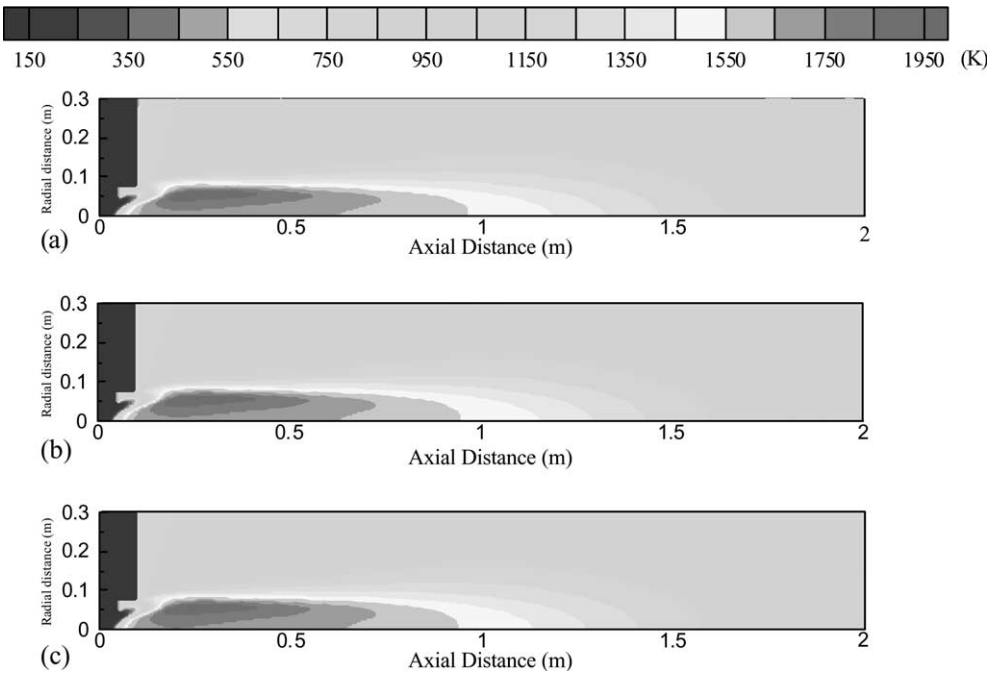

Fig. 13. Predicted isothermal lines for various tertiary air swirl numbers, K. (a) $S_{primary} = 1.38$, $S_{tertiary} = 0.54$; (b) $S_{primary} = 1.38$, $S_{tertiary} = 0.93$ and (c) $S_{primary} = 1.38$, $S_{tertiary} = 1.62$.

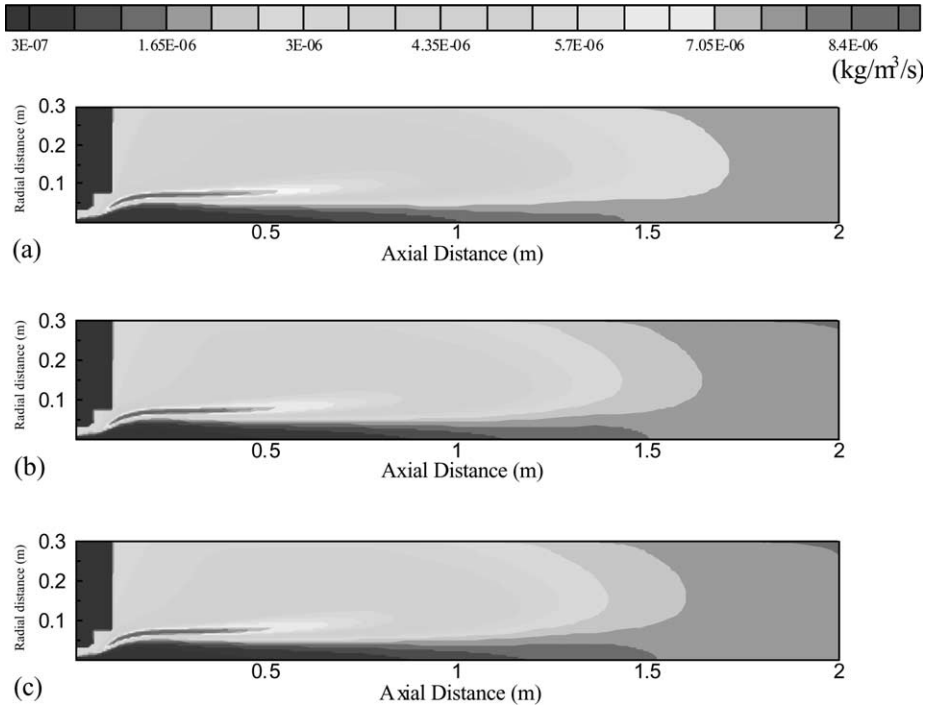

Fig. 15. Production rate of thermal NO for various tertiary air swirl numbers, kg/m^3/s. (a) $S_{primary} = 1.38$, $S_{tertiary} = 0.54$; (b) $S_{primary} = 1.38$, $S_{tertiary} = 0.93$ and (c) $S_{primary} = 1.38$, $S_{tertiary} = 1.62$.

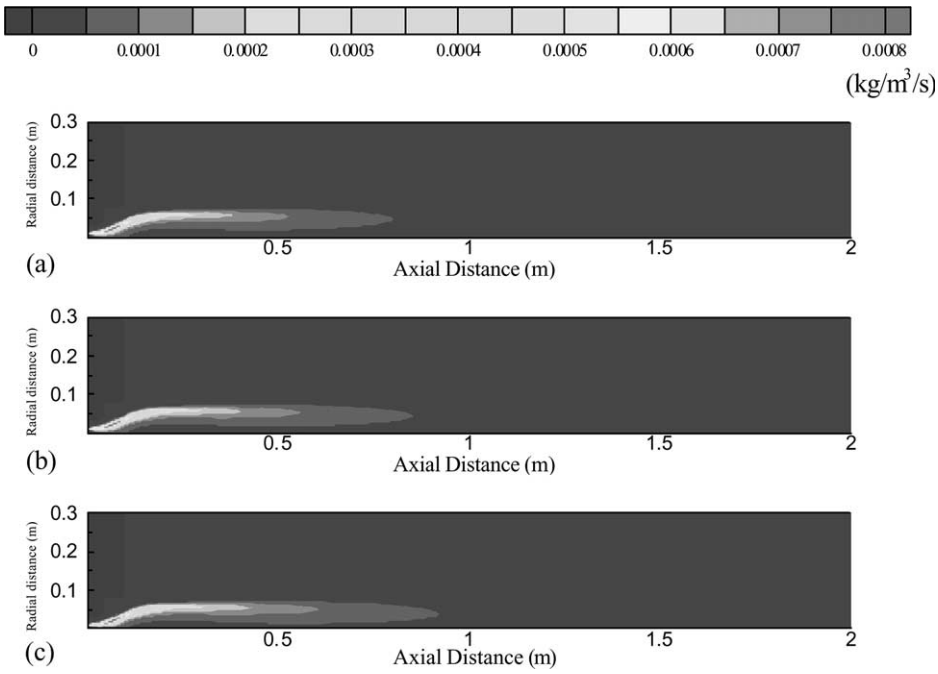

Fig. 16. Production rate of prompt NO for various tertiary air swirl numbers, kg/m^3/s. (a) $S_{primary} = 1.38$, $S_{tertiary} = 0.54$; (b) $S_{primary} = 1.38$, $S_{tertiary} = 0.93$ and (c) $S_{primary} = 1.38$, $S_{tertiary} = 1.62$.

chemical reaction while reducing the gas temperature at exit for the experiments done in this study.

4.3.2. NO formation

The predicted and measured emissions of total NO are compared in Fig. 14 as the tertiary air swirl number is varied. The computed NO emissions, as a whole, show good agreements with the experimental data. As the tertiary air swirl number increases, the total NO emission is observed to slightly decrease. This is due to the fact that the gas temperature at exit becomes lower for higher tertiary swirl number. In a qualitative comparison with the results for heavy fuel oil burner [4], the influence of tertiary air swirl number on NO emission for LPG burner is smaller than that in heavy fuel oil which contains nitrogen compound in itself. However, above results show that the variation of tertiary air swirl number in a combustor is not actually an effective method for reduction of the thermal and prompt NO, because its reduction is not significant.

In Figs. 15 and 16, a spatial distribution of the predicted thermal and prompt NO formation is depicted. There is only a slight change in the formation of thermal NO with the variation of tertiary air swirl number. This results from the fact that there is only a insignificant variation of gas temperature as noted above. In Fig. 16 the region of formation of the prompt NO is seen to be broader with the increment in tertiary air swirl number, which might be due to the enhanced mixing of fuel and tertiary air. However, total production of prompt NO at exit decreases as depicted in Fig. 17. The decrease of the total prompt NO formation is primarily due to the reduction in upstream reaction zone due to enhanced mixing in which prompt NO is primarily formed.

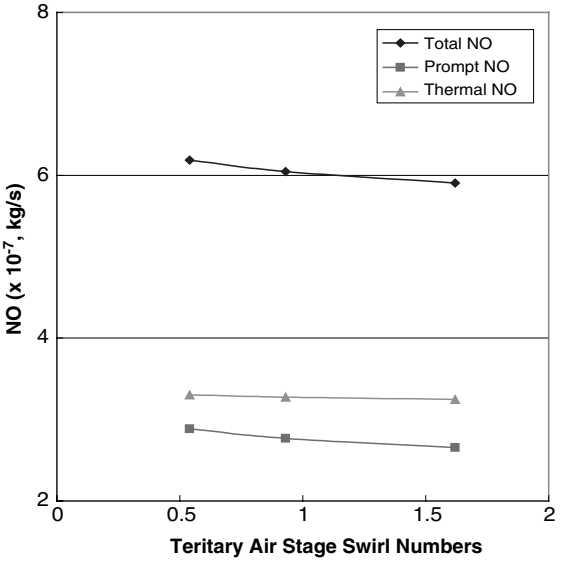

Fig. 17. Total production of thermal prompt NO for various tertiary air swirl numbers, kg/s.

5. Conclusions

In the above, a numerical as well as experimental investigation was performed to predict and measure the thermo-chemical characteristics in an air-staged, swirling LPG flame. The weighted sum of gray gases model for non-gray radiation was combined with the DOM with supplementary boundary conditions to solve the RTE together with the other mass, momentum, energy and species conservation equations. For its validation, a 0.2 MW pilot multi-staged air burner has been designed and constructed. As a result, the formation characteristics of thermal and prompt NO were discussed for various excess air ratios and tertiary air swirl numbers. Some practically meaningful results were obtained by changing the operational conditions.

The formation of thermal NO was found to be more affected by concentration of O_2 and N_2 than gas temperature for a range of excess air ratio studied. The formation of prompt NO decreased as the excess air ratio increased, because of a reduction in reaction zone where the prompt NO was primarily formed. The total formation of NO at exit, however, somewhat increased due to increase in thermal NO even if the prompt NO decreased.

As the tertiary air swirl number increased, the isothermal lines have a little shifted into upstream direction. The formation of the thermal as well as prompt NO at exit was found to decrease slightly. Therefore, a decrease in total NO formation was primarily due to enhanced mixing of fuel and oxygen in the upstream reaction zone and reduced gas temperature at exit.

The current work was performed with gas fuel so that it would be very interesting to examine if these effects still apply to liquid fuel or nitrogen compounded fuel.

Acknowledgement

The financial assistance by the Combustion Engineering Research Center at KAIST is gratefully acknowledged.

References

[1] C.P. Fenimore, Studies of fuel-nitrogen in rich flame gases, Seventeenth Symposium (International) on Combustion, The combustion Institute, 1979, pp. 661–669.

[2] J.P. Smart, R. Webber, Reduction of NO_x and optimisation of burnout with anaerodynamically air-staged burner

and an air-staged precombustor burner, J. Institute Energy (1989) 237–245.
[3] M.A. Toqan, J.M. Beer, P. Jansohn, N. Sun, A. Testa, J.D. Teare, Low NO_x emission from radially stratified natural gas–air turbulent diffusion flames, Twenty-Fourth Symposium on Combustion, The Combustion Institute, 1992, pp. 1391–1397.
[4] A.L. Shihadeh, M.A. Toqan, J.M. Beer, P.F. Lewis, J.D. Teare, J.L. Jimenez, L. Barta, Low NO_x emission from aerodynamically staged oil–air turbulent diffusion flames, ASME Fact. 18 (1994) 195–200.
[5] J.M. Beer, Low NO_x burners for boilers, furnaces and gas turbines; drive towards the lower bounds of NO_x emissions, Combust. Sci. Tech. 121 (1996) 169–191.
[6] N. Sun, Numerical modeling and Experimental Investigation of Radially Stratified Low NO_x Natural Gas Flame, M.S. Thesis, MIT Department of Mechanical Engineering, 1994.
[7] K.Y. Ahn, A Study on the ignition and Combustion of Coal–Water Slury Droplet. Ph.D. Thesis, Korea Advanced Institute of Science and Technology, Taejon, Korea, 1994 (in Korean).
[8] M. Chase Jr., C.A. Davies, J.R. Downey Jr., D.J. Frurip, R.A. Mcdonard, A.N. Syverd, JANAF Thermochemical Tables, third ed., American Chemical Society and American Institute of Physics, 1985.
[9] H.K. Versteeg, W. Malalasekera, An Introduction to Computational Fluid Dynamics, Longman Scientific & Technical, 1995.
[10] A.D. Gosman, F.J.K. Ideriah, TEACH-T: a general computer program for two-dimensional, turbulent recirculating flow, Imperial College, London, UK, 1976.
[11] T.F. Smith, Z.F. Shen, J.N. Friedman, Nov. evaluation of coefficients for the weighted sum of gray gases model, ASME J. Heat Transfer 104 (1982) 602–608.
[12] C.E. Choi, S.W. Baek, Numerical analysis of a spray combustion with nongray radiation using weighted sum gray gases model, Combust. Sci. Tech. 115 (1996) 297–315.
[13] B.F. Magnussen, B.H. Hjertager, On mathematical modeling of turbulent combustion with special emphasis on soot formation and combustion, Sixteenth Symposium (International) on Combustion, The Combustion Institute, 1977, pp. 719–729.
[14] A. Beretta, N. Mancini, F. Podenzani, L. Vigevano, The influence of the temperature fluctuations variance on NO predictions for gas flames, Combust. Sci. Tech. 121 (1996) 193–216.
[15] A.A.F. Peters, R. Weber, Mathematical modeling of 2.25 MW swirling natural gas flame. Part 1: Eddy break-up concept for turbulent combustion; probablity function approach for nitric oxide formation, Combust. Sci. Tech. 110–111 (1995) 67–101.
[16] J.A. Miller, C.T. Bowman, Mechanism and modeling of nitrogen chemistry in combustion, Prog. Energy Combust. Sci. 10 (1989) 287–338.
[17] G. Hand, M. Missaghi, M. Pourkashanain, A. Williams, Experimental studies and computer modeling of nitrogen oxides in a cylindrical natural gas furnace, The IFRF Nineth Members Conference, Noordwijkerhout, The Netherlands, 1989.
[18] M.J. Yu, S.W. Baek, S.J. Kang, Modeling of a pulverized coal combustion with non-gray gas radiation effects, Combust. Sci. Tech 166 (2001) 151–174.
[19] M.C. Drake, S.M. Correa, R.W. Pitz, W. Shyy, C.P. Fenomore, Superequilibrium thermal nitric oxide formation in turbulent diffusion flames, Combust. Flame 69 (1987) 347–365.
[20] G.G. De Soete, Overall reaction rates of NO and N_2 formation from fuel nitrogen. 15th Symposium (Int.) on Combustion/The Combustion Institute 1974, pp. 1093–1112.